Available online at www.sciencedirect.com
ScienceDirect
Trans. Nonferrous Met. Soc. China 25(2015) 533−543
Transactions of Nonferrous Metals Society of China
www.tnmsc.cn

Effect of cooling rates on clustering towards icosahedra in rapidly solidified $Cu_{56}Zr_{44}$ alloy

Yan-jun HU[1,2], Da-dong WEN[1], Yuan-qi JIANG[1], Yong-he DENG[1], Ping PENG[1]

1. School of Materials Science and Engineering, Hunan University, Changsha 410082, China;
2. School of Information Engineering, Guangdong Medical College, Dongguan 523808, China

Received 18 February 2014; accepted 15 July 2014

Abstract: The rapid solidification processes of liquid $Cu_{56}Zr_{44}$ alloys at different cooling rates (γ) were simulated by a molecular dynamics (MD) method. In order to assess the influence of cooling rate on the clustering tendency and degree towards icosahedrons, a ten-indices' cluster-type index method was suggested to characterize the local atomic structures in the super-cooled liquid and the rapidly solidified solid. And their clustering and ordering degrees as well as the packing density of icosahedral clusters were also evaluated by an icosahedral clustering degree (f_I), the chemical order parameter ($\eta_{\alpha\beta}$) and densification coefficients (D_0, D_I and D_{IS}), respectively. Results show that the main local atomic configurations in $Cu_{56}Zr_{44}$ alloy system are Z12 clusters centered by Cu, and most of which are (12 0 12 0 0 0 0 0 0 0) standard icosahedra and (12 0 8 0 0 0 2 2 0 0) as well as (12 2 8 2 0 0 0 0 0 0) defective icosahedra. Below glass transition temperature (T_g), these icosahedral clusters will be coalesced to various icosahedral medium-range orders (IMROs) by IS linkages, namely, icosahedral bond, and their number N, size n, order parameter $\eta_{\alpha\beta}$ as well as spatial distributions vary with γ. As the cooling rate exceeds the critical value (γ_c) at which a glassy transition can take place, a lower cooling rate, e.g., $\gamma_1=10^1$ K/ns, is demonstrated to be favorable to uplift the number of icosahedra and enlarge the size of IMROs compared with the higher cooling rates, e.g., $\gamma_5=10^5$ K/ns, and their packing density and clustering degree towards icosahedra in the rapidly solidified solid can also benefit from the slow cooling process.

Key words: rapid solidification; Cu−Zr alloy; cooling rate; clustering; icosahedron

1 Introduction

Recently, many researchers [1−4] have realized that the glass-forming ability (GFA) of transition metal−transition metal (TM−TM) alloys is intimately correlated with the degree of atomic dense packing in super-cooled liquid and rapidly solidified solid. As a representative of TM−TM metallic glasses (MG), Cu−Zr alloy system has attracted considerable attention due to its simple atomic structure and high GFA over a wide range of compositions [4−7]. Previous investigations indicate that the densely packed atomic structures are always favorable for the formation of glassy phases upon quenching [4], and some short-range orders (SROs) [7] even medium-range orders (MROs) [8] can be identified in super-cooled liquids and rapidly solidified solids. Among the various SROs, icosahedrons with five-fold symmetry are demonstrated to play a key role in the formation of Cu−Zr glassy alloys [7−9], and its strong kinetic constraint on nucleation and subsequent growth of long-range crystalline orders can be attributed to the densely packed atomic structure and a high structural stability [10].

In light of the importance of icosahedrons in the GFA, great efforts have devoted to investigate the microstructures in glassy alloys. Based on the basic ideal of atomic dense packing, several structural models have been proposed, e.g., earlier hard sphere random dense packing model [11] and topological model [12] as well as recent cluster dense packing models [13,14]. However, up to now it is still a challenge to exhibit an explicit structural of amorphous alloys. A well accepted viewpoint is that clusters, i.e., convex polyhedra made up of one central atom and some shell atoms, should be the major building blocks of microstructures in glassy alloys. To identify and characterize these local atomic configurations, Voronoi tessellation technique [15] has

Foundation item: Project (51071065) supported by the National Natural Science Foundation of China; Project (20100161110001) supported by the Specialized Research Fund for the Doctoral Program of Higher Education of China
Corresponding author: Ping PENG; Tel: +86-731-88821727; E-mail: peng@hnu.edu.cn
DOI: 10.1016/S1003-6326(15)63635-4

been widely adopted in previous molecular dynamics (MD) simulation or Monte Carlo (MC) modeling on microstructures of metallic glasses. For example, the Voronoi polyhedron denoted by Voronoi index ⟨0, 0, 12, 0⟩ is a full icosahedron, and the icosahedron-like [10] polyhedrons can be denoted by ⟨0, 2, 8, 2⟩, ⟨0, 3, 6, 3⟩ and ⟨0, 4, 4, 4⟩. Voronoi polyhedrons are good at exploring local geometries and estimating local atomic volumes quickly. However, there are some possibilities of judging the severely distorted icosahedron as the other polyhedron and vice versa [16,17], because the nearest-neighbor atoms around the central atom cannot be clearly defined. Although this miscarriage of justice has been diminished recently by a radical plane technique [16], the geometrical feature between the central atom and its nearest neighbors in identified clusters is scarcely reflected by Voronoi index. For example, the icosahedron-like ⟨0, 2, 8, 2⟩, ⟨0, 3, 6, 3⟩ and ⟨0, 4, 4, 4⟩ polyhedrons are difficult to be distinguished from ⟨0, 0, 12, 0⟩ icosahedrons in terms of their atomic arrangement and symmetry of clusters.

In this work, To identify the basic clusters in binary $Cu_{56}Zr_{44}$ alloys, the nearest-neighbor atoms around the central atom will be exactly extracted by means of partial pair distribution functions $g_{\alpha\beta}(r)$, and a extended cluster-type index method (CTIM) based on the Honeycutt−Andersen (H−A) bond-type index [18] will be adopted to characterize the spatial relationship of the central atom with shell atoms in basic clusters. Special attention will be paid to the identification of icosahedral SRO and MRO clusters in super-cooled liquids and rapidly solidified solids. And the packing density and the ordering degree of icosahedral MRO clusters will be investigated to evaluate the influence of cooling rate on the clustering tendency towards icosahedra in the rapidly solidified solid.

2 Simulation methods

Using a large-scale atomic/molecular massively parallel simulator (LAMMPS) code [19], a MD simulation of the rapid solidification process of liquid $Cu_{56}Zr_{44}$ alloys was carried out, in which 10000 atoms were constructed by randomly distributing 5600 Cu and 4400 Zr atoms in a cubic box subjected to the periodic boundary condition were considered, and their motion equations were solved by Verlet's algorithm in the velocity form with a time step of 1 fs. Constant pressure (p) and temperature (T) were imposed by the modified Nose−Hoover method [20] for both p and T variables and an embedded-atom model (EAM) potential developed recently for the Cu−Zr alloys [21] in a many-body framework was utilized. The $Cu_{56}Zr_{44}$ alloy was initially melted and equilibrated at 1600 K for 1 ns above the experimental melting temperature T_m=1191 K [6], and then was cooled down to 300 K at five different cooling rates ($\gamma_1=10^1$ K/ns, $\gamma_2=10^2$ K/ns, $\gamma_3=10^3$ K/ns, $\gamma_4=10^4$ K/ns and $\gamma_5=10^5$ K/ns). The cooling run was performed in the NPT ensemble without pressure. In our simulation, a primary temperature interval and the isothermal running time at selected temperatures were set as 100 K and 0.1 ps, respectively. Moreover, a temperature interval of 10 K was also adopted to obtain exact data of atomic positions at some special stages of solidification, e.g., the temperatures near by transition of liquid to solid.

3 Results and discussion

3.1 Statistical analysis on microstructures

The pair distribution function $g(r)$ has been widely used to describe the structure characteristics of liquid and solid alloys [1]. Figure 1 plots total $g_{total}(r)$ curves of liquid and rapidly solidified solid $Cu_{56}Zr_{44}$ alloy at different cooling rates. One can see that the first peak of $g(r)$ curves in rapidly solidified solid becomes sharper and the second peak of $g(r)$ curves exhibits a distinct shoulder relative to the liquid, indicating more short-range orders (SRO) even some medium-range orders (MRO) emerge in rapidly solidified solids of 300 K [22,23]. The split second peak and an increasing shoulder in $g(r)$ curves mean that the rapidly solidified solids are of amorphous characteristics [23], and the number of icosahedron-like MROs rises with the decrease of γ in the rapidly solidified solids [24]. That is to say, all cooling rates in this simulation exceed the critical value at which the amorphous solid can be obtained. Figure 2 further illustrates the variation of volume (V) per atom with T in $Cu_{56}Zr_{44}$ alloy system. No abrupt change in V can be observed, indicating the first order phase transitions such as the crystallization are absent [23,25]. It is noticed that below T_m the V at high

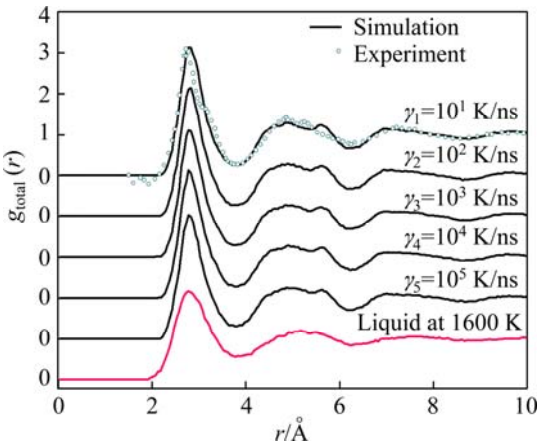

Fig. 1 Total $g(r)$ curves of $Cu_{56}Zr_{44}$ alloys at 300 K and 1600 K (The experimental data are taken from Ref. [5])

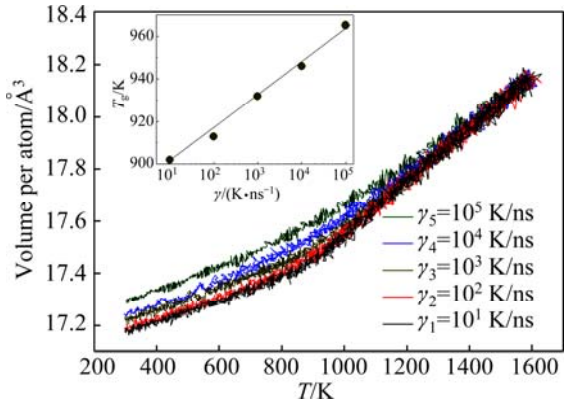

Fig. 2 Volume of $Cu_{56}Zr_{44}$ alloy system per atom as function of temperature (The insert is the cooling rate γ dependence of glass transition temperature T_g)

cooling rates, e.g., $\gamma_5=10^5$ K/ns, is significantly larger than that at low cooling rates, e.g., $\gamma_1=10^1$ K/ns, which implies that increasing γ will lead to the free volume in rapidly solidified solid to go up [9]. From the curve of V vs T, the glass transition temperature (T_g) can be deduced by means of extrapolating and intersecting two linear parts of V vs T curve from 300 K to 1400 K. For $\gamma_1=10^1$ K/ns, $\gamma_2=10^2$ K/ns, $\gamma_3=10^3$ K/ns, $\gamma_4=10^4$ K/ns and $\gamma_5=10^5$ K/ns, the evaluated T_g are 912, 926, 943, 958 and 972 K, respectively, which are higher than the experimental values of 674 K [6], but very close to the simulated results of 940 K in Ref. [26]. As the cooling rate dependence of T_g is further analyzed (see the insert of Fig. 2), a linear variation of T_g with lg γ [27] indicates that the glassy transition of liquid $Cu_{56}Zr_{44}$ alloys is indeed a typical kinetic process [7,27].

Further, based on the total $g(r)$ and partial pair distribution function $g_{\alpha\beta}(r)$ curves at 300 K, Spaepen–Cargill chemical short-range order (CSRO) parameter $\eta_{\alpha\beta}$ [28] is also calculated by the following equations:

$$\eta_{\alpha\beta} = Z_{\alpha\beta} / Z^*_{\alpha\beta} - 1 \quad (1)$$

$$\begin{cases} Z^*_{\alpha\beta} = c_\beta Z_\alpha Z_\beta / \langle Z \rangle \\ \langle Z \rangle = c_\alpha Z_\alpha + c_\beta Z_\beta \end{cases} \quad (2)$$

where α and β represent atomic species, respectively; c_α and c_β denote the concentrations of α and β atoms in simulated system, respectively; $Z_{\alpha\beta}$, Z_α and $\langle Z \rangle$ are the partial, total and average coordination number of Cu or Zr atoms, respectively. The calculated results are listed in Table 1. Table 1 shows that the calculated $Z_{\alpha\beta}$, Z_α and $\langle Z \rangle$ as well as η_{CuZr} are in good agreement with the experimental values reported by MA et al [6]. That is, η_{CuZr} is positive and a little more than 0 in the liquid and rapidly solidified solid of $Cu_{56}Zr_{44}$ alloys, indicating that heterogeneous Cu and Zr atoms tend to bond each other but their ordering degree is not as high as $Pd_{80}Si_{20}$ and $Co_{80}P_{20}$ glassy alloys [28]. With the decrease of temperature T, the η_{CuZr} slightly ascends, and this slight ascent in η_{CuZr} is smaller at higher cooling rates, e.g., $\gamma_5=10^5$K/ns, relative to lower cooling rates, e.g., $\gamma_1=10^1$K/ns, which means that the ordering between Cu and Zr atoms in the $Cu_{56}Zr_{44}$ glassy alloys will benefit from the slow cooling process. Moreover, an average coordination number $\langle Z \rangle \approx 13$ in rapidly solidified solids reveals that these $Cu_{56}Zr_{44}$ glassy alloys are approximately dense packing [4]. However, it is noticed that the total coordination number Z_α of local atomic structures centered by Cu is close to 12 and independent of cooling rates, but the number of heterogeneous atoms in the first coordination shell varies with γ. In the case of $\gamma_1=10$ K/ns, the partial coordination number $Z_{\alpha\beta}$ is 6.58, whereas it is 6.34 at $\gamma_5=10^5$ K/ns. Thus, the majority of local atomic structures with coordination number of 12 (remarked as Z12 hereinafter) can be deduced from the statistical point of view. That is, the local atomic structures in $Cu_{56}Zr_{44}$ glassy alloys are mainly Z12 clusters centered by Cu as well as a few of Z14~Z15 clusters centered by Zr, and the Cu concentration in Cu-centered Z12 clusters varies from 49.2% to 51.0% corresponding to the increase of γ from 10 K/ns to 10^5 K/ns.

Table 1 Partial $Z_{\alpha\beta}$, total Z_α and average $\langle Z \rangle$ coordination number of Cu and Zr in $Cu_{56}Zr_{44}$ alloy at 300 K as well as their Spaepen–Cargill CSRO parameter η_{CuZr}

Temperature/K	γ/(K·ns^{-1})	Z_{CuCu}	Z_{CuZr}	Z_{Cu}	Z_{ZrCu}	Z_{ZrZr}	Z_{Zr}	<Z>	η_{CuZr}	Ref.
1600		5.74	6.06	11.80	7.84	5.76	13.60	12.59	0.081	This work
300	10^1	5.38	6.58	11.96	8.42	6.00	14.42	13.04	0.131	
	10^2	5.39	6.56	11.95	8.41	5.98	14.39	13.02	0.129	
	10^3	5.41	6.54	11.95	8.38	6.00	14.38	13.02	0.126	
	10^4	5.52	6.44	11.96	8.27	6.06	14.33	13.00	0.111	
	10^5	5.59	6.34	11.93	8.15	6.11	14.26	12.96	0.098	
300		4.54	6.45	10.99	8.22	6.05	14.27	12.43	0.162	Experiment [6]

3.2 Characterization of basic clusters

The coordination number reflects atom distribution in statistical average but cannot describe the local atomic configuration. Honeycutt−Andersen (H−A) bond-type index [18] was proved to be successful in assessing local configurations of liquid and amorphous alloys [25]. In this pair analysis technique, two atoms are regarded to be near-neighbors and form a bond if they are within a specified cutoff distance. Here, the cutoff distance corresponds to the first minimum r_{min} in partial $g_{\alpha\beta}(r)$ curves. A sequence of four integers (*ijkl*) are designed to describe the different local configurations. The first integer *i* is a remark of the bonding between two given atoms. *i* is 1 when the atoms in the root pair are bonded, otherwise *i* is 2. The second integer *j* is the number of near-neighbor atoms shared in common by the root pair. The third integer *k* is the number of bonds among the shared neighbors. The fourth integer *l* is needed to distinguish configurations with same first three indices but different bonding geometries. This method is convenient to characterize and analyze the geometric characteristics of basic clusters. For example, 1551 bond-pair represents two root pair atoms with five common neighbors, among which five bonds form a pentagon by near-neighbor contact, as shown in Fig. 3. In this case, some typical bonded pairs are examined for understanding the local structure of systems. For example, the number of 1551 bond-pairs with five-fold symmetry is a measure of the degree of ideal icosahedral short-range order [25]. 1421 and 1422 bond-pairs are characteristic bond-pairs of FCC and HCP crystal structures, respectively. 1661 and 1441 bond-pairs are characteristic bond pairs of BCC crystal structure [29].

As an example, Table 2 lists the variation of various H−A bond-types with *T* in $Cu_{56}Zr_{44}$ alloy system at $\gamma_1=10^1$ K/ns. It is noticed that 1551, 1541 and 1431 bond-types closely related to icosahedra account for about 56.6% and 72.1% of the total number at 1600 K and 300 K, respectively, and the sum of 1551, 1541, 1431, 1661, 1441, 1442, 1421, 1331 and 1321 is 95% and over below T_m. In contrast, each of 1651, 1301, 1411, 1531, 1532, 1771, 1201 and 1211 bond-types is not more than 1% and their sum is less than 5%, especially in rapidly solidified solid of 300 K. Hence, it can be concluded that 1651, 1301, 1411, 1531, 1532, 1771, 1201 and 1211 do not belong to the characteristic bond-types of $Cu_{56}Zr_{44}$

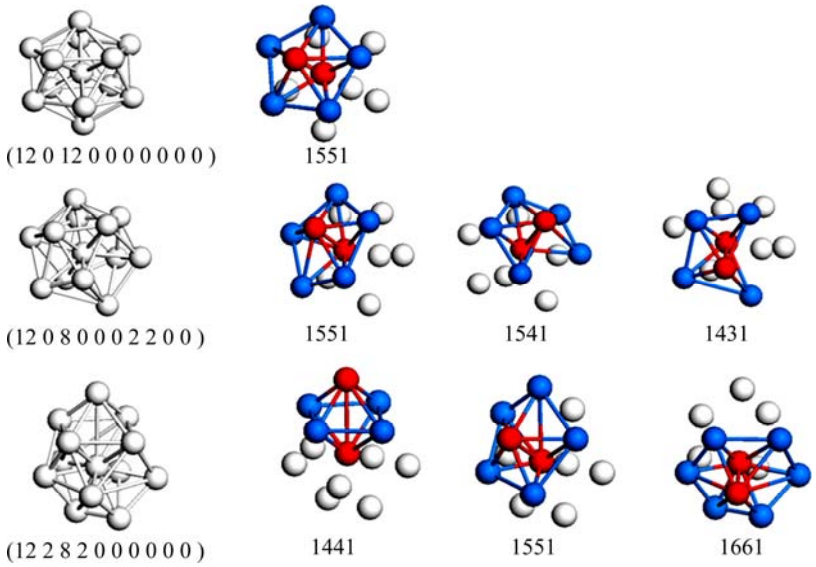

Fig. 3 Schematic diagrams of H−A bond-types in standard and defective icosahedrons (The red balls and blue balls represent root pair atoms and near-neighbor atoms shared in common by the root pair, respectively. The red and blue lines denote the bond between the root pair atoms and bonds among the shared neighbors, respectively)

Table 2 Relative number of various H−A bond-types in rapidly solidified $Cu_{56}Zr_{44}$ alloy system at $\gamma_1=10^1$ K/ns

T/K	Major/%										Minor/%							
	1551	1541	1431	1661	1441	1422	1421	1311	1321	Sum	1651	1301	1411	1531	1532	1771	1201	1211
300	42.3	16.1	13.7	11.0	6.4	4.8	1.5	1.3	1.0	98.1	0.4	0.4	0.3	0.3	0.2	0.1	0.1	0.0
800	40.1	16.4	14.3	10.7	6.6	4.6	1.6	1.7	1.6	97.6	0.6	0.4	0.3	0.4	0.4	0.1	0.1	0.1
910	39.1	16.5	14.8	10.7	6.6	4.5	1.6	1.8	1.8	97.4	0.7	0.4	0.3	0.4	0.4	0.1	0.1	0.1
1100	30.9	17.7	16.7	10.2	7.4	5.3	2.1	2.7	2.8	95.8	1.0	0.7	0.5	0.7	0.7	0.2	0.3	0.2
1600	19.5	17.5	19.6	8.20	7.5	6.4	3.0	4.9	5.7	92.3	1.8	0.7	0.7	1.2	1.2	0.3	0.8	0.7

alloy system. In this alloy system, the major bond-types are 1551, 1541, 1431, 1661, 1441, 1421, 1422 1331 and 1321.

To characterize topological structures of basic clusters aggregated by a group of the nearest-neighbor atoms, a developed cluster-type index method (CTIM) [17] is adopted. Herein, ten integers (Z, n_1, n_2, n_3, n_4, n_5, n_6, n_7, n_8, n_9) are assigned to denote different types of basic clusters which are defined as a group of atoms bound together with a central atom as the core surrounded by the nearest-neighbor atoms. Z is the coordination number of the central atom. n_1, n_2, n_3, n_4, n_5, n_6, n_7, n_8 and n_9 denote numbers of 1441, 1551, 1661, 1421, 1422 1541, 1431, 1321 and 1311 bond-types formed between surrounding atoms and the central atom, respectively. Since all major bond-types in $Cu_{56}Zr_{44}$ alloy system are taken into account in the present of CTIM, undoubtedly, it should be sufficient for characterizing local atomic configurations of liquid and rapidly solidified solid. In fact, it is found that other basic clusters such as Frank–Kasper polyhedrons, Bernal polyhedrons as well as characteristic clusters of FCC, BCC and HCP crystals may be also identified by this ten indices' CTIM. For example, (12 0 12 0 0 0 0 0 0 0) denotes a standard Z12 icosahedron constructed by one central atom and 12 neighbor atoms. (8 4 4 0 0 0 0 0 0 0), (9 3 6 0 0 0 0 0 0 0) and (10 2 8 0 0 0 0 0 0 0) stand for Bernal polyhedrons of Z8 tetragonal dodecahedron, Z9 tri-capped trigonal prism and Z10 bi-capped square Archimedean ant-prism [1], respectively. Other canonical Frank–Kasper polyhedra [30] with Z11, Z13, Z14, Z15, Z16 and Z17 can be remarked as (11 2 8 1 0 0 0 0 0 0), (13 1 10 2 0 0 0 0 0 0), (14 0 12 2 0 0 0 0 0 0), (15 0 12 3 0 0 0 0 0 0), (16 0 12 4 0 0 0 0 0 0) and (17 0 12 5 0 0 0 0 0 0) , respectively. (12 0 0 0 6 6 0 0 0 0), (12 0 0 0 12 0 0 0 0 0) and (14 6 0 8 0 0 0 0 0 0) represent Z12 HCP, Z12 FCC and Z14 BCC clusters [29], respectively. Z6 octahedron and Z7 icosahedron can be represented as (6 6 0 0 0 0 0 0 0 0) and (7 5 2 0 0 0 0 0 0 0), respectively.

By means of this developed CTIM, the basic clusters in $Cu_{56}Zr_{44}$ alloy system can be conveniently identified. Over 30 species of basic clusters are detected in present simulated system, among which only 15 species are found to be more than 30 in quantity. Figure 4 illustrates the variation of number of typical basic clusters with cooling rate in the liquid of 1200 K and the rapid solidification solid of 300 K. It is found that the number of basic clusters in the rapid solidification solid seldom varies with γ except for (12 0 12 0 0 0 0 0 0 0) and (12 0 8 0 0 0 2 2 0 0). As elaborated above, (12 0 12 0 0 0 0 0 0 0) is a standard icosahedron associated by twelve 1551 bond-pairs. As one bond between a pair of outer atoms in an icosahedron being broken, four 1551

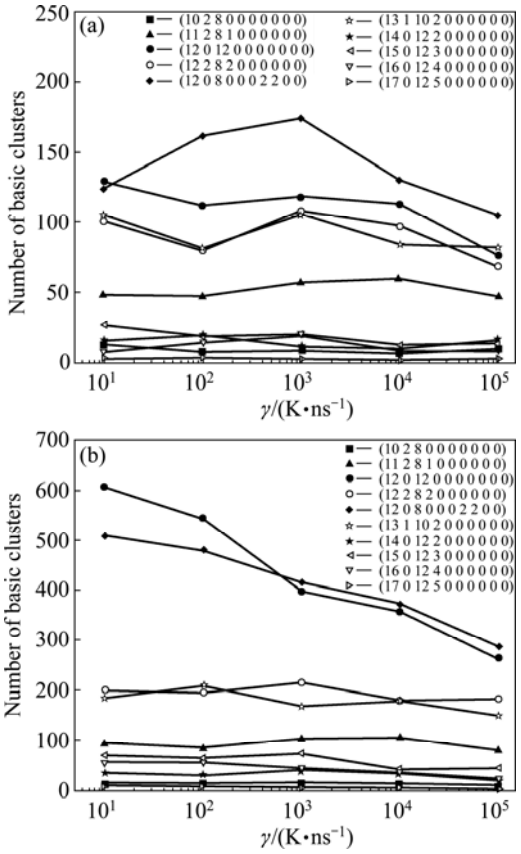

Fig. 4 Cooling rate γ dependence of number of basic clusters in liquid of 1200 K (a) and rapid solidified solid of 300 K (b)

bond-pairs will transform into two 1541 bond-pairs and two 1431 bond-pairs [25], and then the icosahedron with four breakings of 1551 bond-pairs will change into (12 0 8 0 0 0 2 2 0 0). Since the majority of bond-types in (12 0 8 0 0 0 2 2 0 0) are still 1551 with five-fold symmetry, it is usually called as a defective icosahedron [25]. Another common defective icosahedron is (12 2 8 2 0 0 0 0 0 0) [31], in which four 1551 bond-pairs are replaced by two 1441 and two 1661 bond-pairs. Table 3 further lists the number of typical Z12 basic clusters at various cooling rates. It is found that most Z12 basic clusters are (12 0 12 0 0 0 0 0 0 0) standard icosahedra as well as (12 0 8 0 0 0 2 2 0 0) and (12 2 8 2 0 0 0 0 0 0) defective icosahedra, which means that icosahedral clusters indeed play a critical role in the formation of $Cu_{56}Zr_{44}$ metallic glass [7]. A further analysis shows that the icosahedral clusters with Z12 and their defective configurations with Z11 or Z13 are centered by smaller Cu atoms (R_{Cu}=128 pm), while other basic clusters with Z14, Z15, Z16 and Z17 are centered by bigger Zr atoms (R_{Zr}=160 pm). And the chemical composition of (12 0 12 0 0 0 0 0 0 0) icosahedra and (12 0 8 0 0 0 2 2 0 0) defective icosahedra is mainly Cu_7Zr_6, Cu_6Zr_7 and Cu_5Zr_8 at 300 K, among which Cu_7Zr_6 is the most popular (see Fig. 5).

Table 3 Number of typical *Z*12 basic clusters in $Cu_{56}Z_{44}$ alloy system at various cooling rates (The values in parentheses denote the number of Zr-centered basic clusters)

Type	300 K					1200 K				
	10^1 K/ns	10^2 K/ns	10^3 K/ns	10^4 K/ns	10^5 K/ns	10^1 K/ns	10^2 K/ns	10^3 K/ns	10^4 K/ns	10^5 K/ns
(12 0 12 0 0 0 0 0 0 0)	607(3)	544(3)	397(4)	357(2)	263(6)	129(2)	112(0)	118(3)	113(1)	76(1)
(12 2 8 2 0 0 0 0 0 0)	198(1)	195(0)	214(1)	178(1)	180(0)	101(1)	79(0)	108(2)	97(1)	68(2)
(12 3 6 3 0 0 0 0 0 0)	63(0)	64(0)	75(0)	62(0)	89(0)	67(2)	45(0)	60(0)	53(1)	48(1)
(12 4 4 4 0 0 0 0 0 0)	11(0)	19(0)	21(0)	18(1)	24(0)	16(1)	9(0)	15(0)	13(0)	19(0)
(12 0 8 0 0 0 2 2 0 0)	509(6)	480(1)	416(2)	373(4)	287(5)	124(2)	162(3)	174(3)	130(2)	105(0)
(12 0 7 0 0 0 2 2 1 0)	80(0)	58(1)	40(3)	66(3)	48(1)	39(2)	33(0)	34(3)	43(4)	31(1)
(12 0 6 0 0 2 2 2 0 0)	92(0)	94(4)	86(3)	76(4)	70(3)	26(1)	32(1)	30(0)	35(2)	59 (0)
(12 0 5 0 1 0 3 3 0 0)	87(2)	61(2)	63(0)	73(2)	71(2)	29(2)	45(1)	36(3)	38(1)	19(1)
(12 2 5 1 0 0 3 1 0 0)	111(1)	79(0)	108(1)	89(0)	83(1)	73(0)	61(2)	59(3)	57(0)	49(2)
(12 2 4 2 0 0 2 2 0 0)	120(0)	110(0)	121(1)	134(0)	115(0)	105(1)	104(3)	92(1)	95(3)	87(1)
(12 0 4 0 0 0 4 4 0 0)	52(1)	57(0)	60(0)	70(1)	54(2)	37(0)	28(3)	35(2)	27(1)	32(0)
(12 0 3 0 1 2 3 3 0 0)	42(0)	49(4)	29(1)	35(2)	38(0)	14(2)	27(1)	16(1)	14(0)	21(0)
Sum	1972(14)	1810(15)	1630(16)	1531(20)	1322(20)	760(16)	737(14)	777(21)	715(16)	614(9)

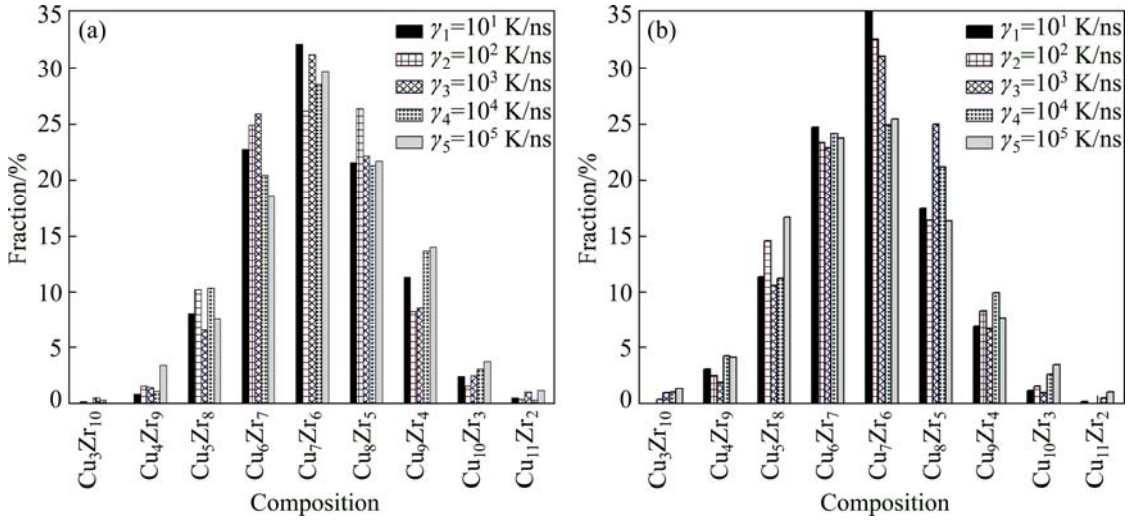

Fig. 5 Chemical composition of (12 0 12 0 0 0 0 0 0 0) icosahedra (a) and (12 0 8 0 0 0 2 2 0 0) defective icosahedra (b) at 300 K

3.3 Icosahedral medium-order

Basic clusters can be linked by vertex sharing (VS), edge-sharing (ES), face-sharing (FS) and intercross-sharing (IS) atoms [29]. In this case, extended clusters with some long-range order will be formed. Figure 6(a) illustrates the configuration of various linkages between two (12 0 12 0 0 0 0 0 0 0) standard icosahedral basic clusters, in which only central atoms in the IS linkage are bonding each other. Figure 7 further plots the cooling rate dependence of number of isolated and extended icosahedra in the liquid of 1200 K and the rapidly solidified solid of 300 K. It is noticed that the icosahedral clusters at 1200 K are mainly isolated icosahedra; however, more icosahedral clusters are coalesced to extended icosahedra at 300 K, and the IS linkage is dominant among four sharing linkages. As previously defined [32], the existence of bond-pairs between central atoms of basic clusters can be adopted to distinguish a medium-range order from extended clusters. Hence, only an extended icosahedral cluster associated by IS linkage, i.e., icosahedral bond [33], can be regarded as the icosahedral medium-range order (IMRO). Similarly to previous results [32], these clusters usually occur in the form of ring, chain or dendrite, and each IMRO corresponds to a specific IS linkage form of central atoms of icosahedra, e.g., chain-shaped double icosahedron with 19 atoms and string-like IMRO assembled by three IS linkages (see Fig. 6(b)).

Table 4 lists the number and size distribution of several typical IMRO clusters in the liquid of 1200 K and the rapidly solidified solid of 300 K. Figure 8 further exhibits their spatial distribution at various cooling rates.

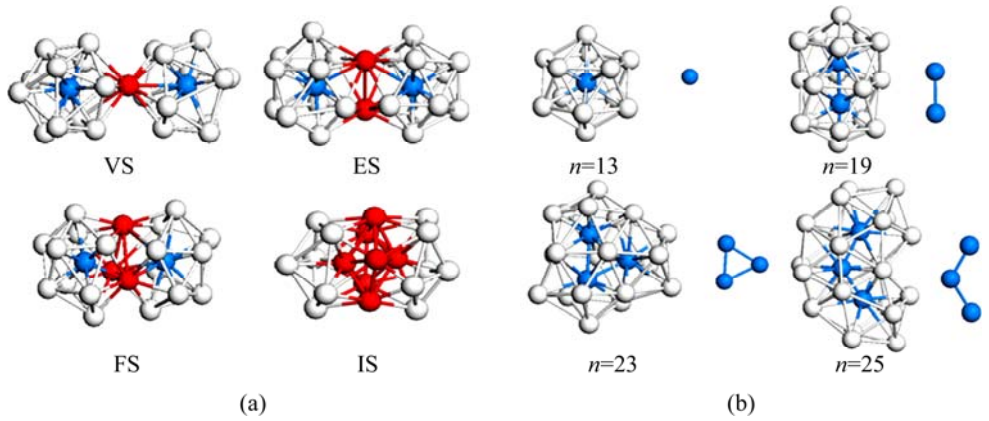

Fig. 6 Schematic diagrams of VS, ES, FS and IS linkages between two icosahedras (a) and typical IMRO clusters (b) (Red and blue balls represent shared atoms and central atoms of icosahedra, respectively. The aggregation of blue lines and blue spheres denotes IS linkages between icosahedra)

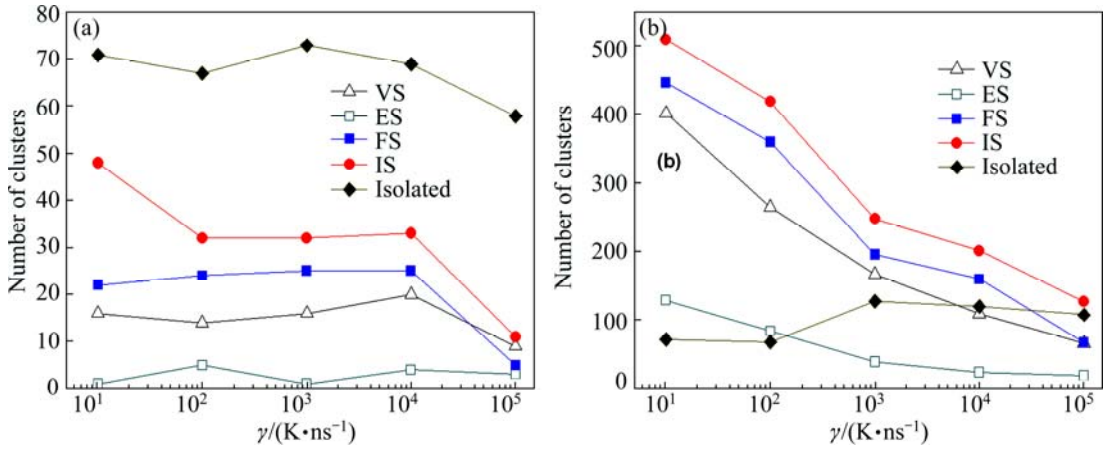

Fig. 7 Cooling rate γ dependence of number of isolated icosahedra and extended icosahedra linked by VS, ES, FS and IS modes in liquid of 1200 K (a) and rapidly solidified solid of 300 K (b)

Table 4 Number and size distribution of several typical IMRO clusters in liquid of 1200 K and rapidly solidified solid of 300 K (N^i is number of the i type IMRO cluster with n^i atoms. N_I^i and N_{IS}^i are number of central atoms and IS linkages in the i type IMRO cluster, respectively)

N_I^i	n^i	N_{IS}^i	N_{IS}^i/N_I^i	N_{IS}^i/n^i	N_I^i/n^i	N^i (300 K)					N^i (1200 K)				
						γ_1	γ_2	γ_3	γ_4	γ_5	γ_1	γ_2	γ_3	γ_4	γ_5
1	13	0	0	0	0.08	94	118	127	119	107	71	67	73	69	58
2	19	1	0.5	0.05	0.11	45	41	39	28	31	10	10	10	11	6
3	23	3	1	0.13	0.13	11	2	4	4	6	1	0	0	0	1
	25	2	0.67	0.08	0.12	16	18	9	18	8	4	4	4	2	1
4	26	6	1.5	0.23	0.15	1	1	0	0	0	0	0	0	0	0
	27	5	1.25	0.19	0.15	3	1	1	1	2	1	1	1	0	0
	29	4	1	0.14	0.14	6	6	4	6	2	1	0	0	0	0
	31	3	0.75	0.10	0.13	7	3	3	6	2	1	0	1	1	0
5	29	9	1.8	0.31	0.17	1	0	0	0	0	0	0	0	0	0
	30	8	1.6	0.27	0.17	0	0	0	1	0	0	0	0	0	0
	33	6	1.2	0.18	0.15	0	2	1	0	1	1	1	1	0	0
	34	5	1	0.15	0.15	0	0	0	1	0	0	0	0	0	0
	35	5	1	0.14	0.14	6	2	2	3	1	0	0	0	0	0
	36	4	0.8	0.11	0.14	1	0	0	0	0	0	0	0	0	0
	37	4	0.8	0.11	0.14	5	4	1	1	1	0	0	0	0	0

One can see that only a double icosahedron and 24 isolated icosahedrons randomly distribute in the initial liquid alloy. With the decrease of temperature, a part of isolated icosahedras gradually aggregate into IMRO clusters [33], and their number N and size n vary with γ. At γ_5=10^5 K/ns, the largest IMRO is a coalescence of 7 icosahedra by 43 atoms, and only 56 IMRO clusters can be detected, whereas they are 122 IMRO clusters and a aggregation of 21 icosahedra by 105 atoms at γ_1=10^1 K/ns. Obviously, the low γ is profitable for the formation and growth of IMRO clusters during the rapid solidification [24]. In this case, a long string-like IMRO backbone, i.e., an interpenetration network of IS linkages [33], will emerge in the rapidly solidified $Cu_{56}Zr_{44}$ alloys, referring to Fig. 8.

3.4 Clustering towards icosahedra

To assess the effect of cooling rate on the clustering degree and the packing density of icosahedral clusters in the rapidly solidified $Cu_{56}Zr_{44}$ alloy, the icosahedral clustering degree (f_I) in the liquid of 1600 K and the rapidly solidified solid of 300 K as well as the densification coefficients (D_0, D_I and D_{IS}) at various cooling rates are further evaluated by following expressions:

$$f_I = (\sum_i N^i \cdot n^i + 13N_{Iso}) / \sum (n_{Cu} + n_{Zr}) \quad (3)$$

$$D_0 = \sum_i N^i \cdot N_I^i / \sum_i N^i \cdot n^i \quad (4)$$

$$D_{IS} = \sum_i N^i \cdot N_{IS}^i / \sum_i N^i \quad (5)$$

$$D_I = \sum_i N^i \cdot N_I^i / \sum_i N^i \quad (6)$$

where N^i is the number of the i type IMRO cluster with n^i atoms; N_I^i and N_{IS}^i are the numbers of central atoms and IS linkages in the i type IMRO cluster, respectively; N_{Iso} is the number of isolated icosahedral clusters with 13 atoms; $\sum(n_{Cu}+n_{Zr})$ is the total number of Cu and Zr atoms in $Cu_{56}Z_{44}$ alloy system. Undoubtedly, the ratio f_I can represent the clustering degree of atoms towards icosahedrons in simulated system to some extent. A high f_I means that more Cu and Zr atoms are aggregated into icosahedra during the rapid solidification of $Cu_{56}Zr_{44}$ alloys. A careful calculation shows that the f_I is very low in the initial liquid. Only 3.3% atoms participate in the construction of icosahedral clusters at 1600 K. With the decrease of temperature, the f_I value ascends steeply. At 300 K, more than a quarter even half of atoms are found to join into icosahedra. As for the influence of cooling rates, Fig. 9 exhibits that the f_I varies rapidly with γ at 300 K, and the f_I value at high γ is far smaller than that at low γ. As well-known, an obvious rise in the number N^i of icosahedral clusters usually takes place at temperature

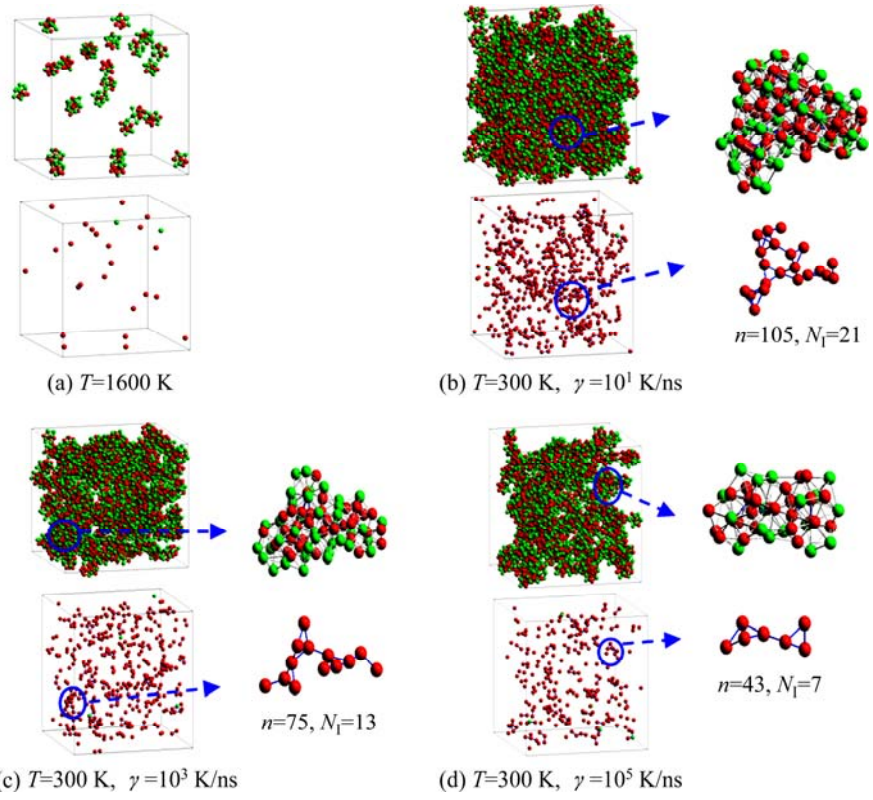

Fig. 8 Spatial distribution of isolated icosahedra and IMRO clusters as well as their central atoms in equilibrium liquid of 1600 K and rapid solidified solids of 300 K at various cooling rates (The region remarked by circle is the largest IMRO. Red and green balls represent Cu and Zr atoms in $Cu_{56}Zr_{44}$ alloy system, respectively)

nearby T_g [7], and the increasing N^i at T_g mainly arises from the coalescence of atoms and clusters as well as the transformation of other polyhedrons to icosahedra [32]. Hence, it is unsurprising that a large f_I emerges at low cooling rates above the critical value rather than at high cooling rates, because an adequate diffusion of solute atoms at low T_g related to low γ is in favor of the aggregation of isolated atoms and the association of isolated atoms with smaller clusters [1].

With regard to the packing density of icosahedral clusters, from Fig. 6 one can see that the numbers of icosahedra and IS linkages in the double icosahedrons with 19 atoms are 2 and 1, respectively. With the enlargement of IMRO clusters from n=19 to n=23 and n=25, the icosahedral bonds become a ring-like network even a string-like backbone. In this case, their icosahedrons N_I and IS linkages N_{IS} are increased to 3, 3 and 3, 2, respectively. As defined above, their densification coefficients (D_0, D_{IS} and D_I) can be calculated. That is, D_0=2/19, D_{IS}=1 and D_I= 2 as n=19, while D_0, D_{IS} and D_I are 3/23, 3, 3 and 3/25, 2, 3, respectively, corresponding to n=23 and n=25. Obviously, the densely packed IMRO cluster with n=23 has larger D_0, D_{IS} and D_I values compared with the loosely packed IMRO cluster with n=25, hence, the magnitude of D_0, D_{IS} and D_I can be adopted to represent the atomic packing density of icosahedral clusters to some extent.

Considering the existence of numerous IMRO clusters with various IS linkages in the rapidly solidified $Cu_{56}Zr_{44}$ alloy as well as their random distribution in the simulated system (see Fig. 8), an average densification coefficient of IMRO clusters is further calculated. Figure 9 plots the γ dependence of the densification coefficients (D_0, D_I and D_{IS}) of the rapidly solidified $Cu_{56}Zr_{44}$ alloy. From Fig. 9, one can see that the cooling rate γ has a significant influence on the atomic packing density of IMRO clusters. With the increase of γ, the D_0, D_I and D_{IS} abruptly decline. At γ=10^1 K/ns, about 14.8% atoms are central atoms in IMRO clusters and there are 4.0 icosahedral bonds and 4.2 icosahedras per IMRO cluster, while the percent of central atoms and the number of icosahedral bonds and icosahedra are merely 12.5%, 2.3 and 2.8, respectively, at γ=10^5 K/ns. Relative to γ_1=10^1 K/ns, the D_0, D_{IS} and D_I at γ_5=10^5 K/ns descend by 2.3%, 1.7 and 1.4, respectively, which indicates that an increasing γ is indeed disadvantageous for the clustering towards icosahedrons. In this case, not only a great deal of the free volumes [34] exist in simulated system (see Fig. 2), but the atomic packing [10,29] is also incompact in IMRO clusters.

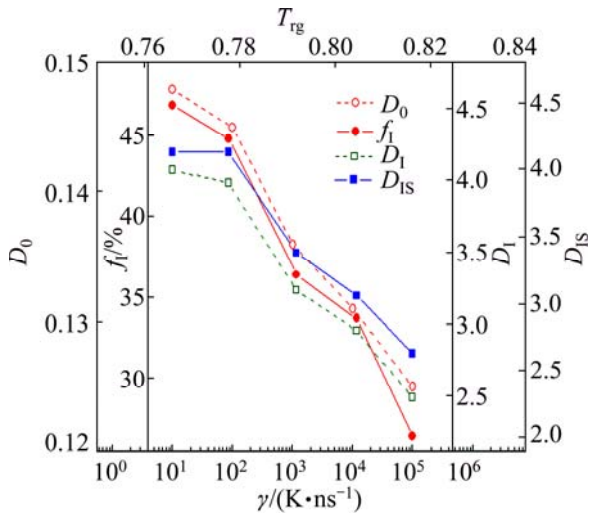

Fig. 9 Cooling rate γ dependence of icosahedral clustering degree f_I and densification coefficients D_0, D_I, D_{IS} of IMRO clusters in rapidly solidified solid of 300 K (T_{rg}=T_g/T_m is the reduced glassy transition temperature of $Cu_{56}Zr_{44}$ alloys)

4 Conclusions

1) A ten-indices' CTIM is sufficient and suitable for the characterization of the basic clusters in present TM−TM alloys. Either in liquid or in solid, heterogeneous Cu and Zr atoms tend to bond each other, but their ordering degree $\eta_{\alpha\beta}$ is much lower relative to transition metal−metalloid metallic (TM−M) glasses.

2) For the rapidly solidified solids, their main local atomic configurations are revealed to be Cu-centered Z12 clusters, and most of which are (12 0 12 0 0 0 0 0 0 0) standard icosahedra and (12 0 8 0 0 0 2 2 0 0) as well as (12 2 8 2 0 0 0 0 0 0) defective icosahedra. Above T_g, these icosahedrons generally emerge in the form of isolated Cu_7Zr_6, Cu_6Zr_7 and Cu_5Zr_8 basic clusters, whereas they can be coalesced to icosahedral medium-range order (IMRO) clusters by IS linkages in the rapidly solidified solids of 300 K.

3) With increasing cooling rate, the quantity N_{Iso} of (12 0 12 0 0 0 0 0 0 0) and (12 0 8 0 0 0 2 2 0 0) basic clusters, the size n^i and number N^i of IMRO clusters remarkably descend at 300 K. Although a high cooling rate can uplift the T_g of $Cu_{56}Zr_{44}$ alloys, a careful analysis on the icosahedral clustering degree and the densification coefficients (D_0, D_I and D_{IS}) indicates a slow cooling is favorable for the clustering towards icosahedrons and their dense packing in the rapidly solidified solid.

References

[1] CHENG Y Q, MA E. Atomic-level structure and structure–property relationship in metallic glasses [J]. Progress in Materials Science, 2011, 56: 379−473.

[2] XU B C, XUE R J, ZHANG B. Superior glass-forming ability and its correlation with density in Ce−Ga−Cu ternary bulk metallic glasses [J]. Intermetallics, 2013, 32: 1−5.

[3] MIRACLE D B.The density and packing fraction of binary metallic glasses [J]. Acta Materialia, 2013, 61: 3157−3171.

[4] LI Y, GUO Q, KALB J A, THOMPSON C V. Matching glass-forming ability with the density of the amorphous phase [J]. Science, 2008, 322: 1816−1819.

[5] LIU X J, XU Y, LU Z P, HUI X, CHEN G L, ZHENG G P, LIU C T. Atomic packing symmetry in the metallic liquid and glass states [J]. Acta Materialia, 2011, 59: 6480−6488.

[6] MA D, STOICA A D, WANG X L, LU Z P, XU M, KRAMER M. Efficient local atomic packing in metallic glasses and its correlation with glass-forming ability [J]. Physical Review B, 2009, 80: 014202.

[7] CHENG Y Q, SHENG H W, MA E. Relationship between structure, dynamics, and mechanical properties in metallic glass-forming alloys [J]. Physical Review B, 2008, 78: 014207.

[8] LIU A C Y, NEISH M J, STOKOL G, BUCKLEY G A, SMILLIE L A, JONGE DE M D, OTT R T, KRAMER M J, BOURGEOIS L. Systematic mapping of icosahedral short-range order in a melt-spun $Zr_{36}Cu_{64}$ metallic glass [J] Physical Review Letters, 2013, 110: 205505.

[9] CHENG Y Q, MA E. Indicators of internal structural states for metallic glasses: Local order, free volume, and configurational potential energy [J]. Applied Physics Letters, 2008, 93: 051910.

[10] YANG L, GE T, GUO G Q, HUANG C L, MENG X F, WEI S H, CHEN D, CHEN L Y. Atomic and cluster level dense packing contributes to the high glass-forming ability in metallic glasses [J]. Intermetallics, 2013, 34: 106−111.

[11] BERNAL J D. Geometry of the structure of monatomic liquids [J]. Nature, 1960, 185: 68−70.

[12] EGAMI T, WASEDA Y. Atomic size effect on the formability of metallic glasses [J]. Journal of Non-Crystalline Solids, 1984, 64: 113−134.

[13] MIRACLE D B. A structural model for metallic glasses [J] Nature Materials, 2004, 3: 697−702.

[14] SHENG H W, LUO W K, ALAMGIR F M, BAI J M, MA E. Atomic packing and short-to-medium range order in metallic glasses [J]. Nature, 2006, 439: 419−425.

[15] FINNEY J L. Random packings and the structure of simple liquids I. The geometry of random close packing [J]. Proceeding the Royal Society of London A, 1970, 319: 479−493.

[16] PARK J, SHIBUTANI Y. Effects of atomic size for voronoi tessellation technique on binary and ternary systems of metallic glasses [J]. Materials Transactions, 2006, 47: 2904−2909.

[17] TIAN Z A, LIU R S, DONG K J, YU A B. A new method for analyzing the local structures of disordered systems [J]. Europhysics Letters, 2011, 96: 36001.

[18] HONEYCUTT J D, ANDEMEN H C. Molecular dynamics study of melting and freezing of small Lennard−Jones clusters [J]. The Journal of Physical Chemistry, 1987, 91: 4950−4963.

[19] PLIMPTON S. Fast parallel algorithms for short-range molecular dynamics [J]. Journal of Computatinal Physics, 1995, 117: 1−19.

[20] MARTYNA G J, TOBIAS D J, KLEIN M L. Constant pressure molecular dynamics algorithms [J]. The Journal of Physical Chemistry, 1994, 101: 4177−4189.

[21] MENDELEV M I, SORDELET D J, KRAMER M J. Using atomistic computer simulations to analyze X-ray diffraction data from metallic glasses [J]. Journal of Applied Physics, 2007, 102: 043501.

[22] KELTON K F, LEE G W, GANGOPADHYAY A K, HYERS R W, RATHZ T J, ROGERS J R, ROBINSON M B, ROBINSON D S. First X-ray scattering studies on electrostatically levitated metallic liquids: Demonstrated influence of local icosahedral order on the nucleation barrier [J]. Physical Review Letters, 2003, 90: 195504.

[23] ZHANG Y, MATTERN N, ECKERT J. Atomic structure and transport properties of $Cu_{50}Zr_{45}Al_5$ metallic liquids and glasses: Molecular dynamics simulations [J]. Journal of Applied Physics, 2011, 10: 093506.

[24] LI M Z, WANG C Z, HAO S G, KRAMER M J, HO K M. Structural heterogeneity and medium-range order in Zr_xCu_{100-x} metallic glasses [J]. Physical Review B, 2009, 80: 184201.

[25] QI L, DONG L F, ZHANG S L, CUI Z Q, MA M Z, JING Q, LI G, LIU R P. Glass formation and local structure evolution in rapidly cooled $Pd_{55}Ni_{45}$ alloy melt: Molecular dynamics simulation [J]. Computational Materials Science, 2008, 42:713−716.

[26] MENDELEV M I, KRAMER M J, OTT R T, SORDELET D J. Molecular dynamics simulation of diffusion in supercooled Cu−Zr alloys [J]. Philosophical Magazine, 2009, 89: 109−126.

[27] ZHANG Y, MATTERN N, ECKERT J. Study of direct relationship between atomic structures and glass forming abilities of $Cu_{100-x}Zr_x$ ($0\leq x\leq 10$) liquids by molecular dynamics simulations [J] Journal of Applied Physics, 2012, 111: 053520.

[28] CARGILL G S, SPAEPEN F. Description of chemical ordering in amorphous alloys [J]. Journal of Non-Crystalline Solids, 1981, 43: 91−97.

[29] HUI X, FANG H Z, CHEN G L, SHANG S L, WANG Y, QIN J Y, LIU Z K. Atomic structure of $Zr_{41.2}Ti_{13.8}Cu_{12.5}Ni_{10}Be_{22.5}$ bulk metallic glass alloy [J]. Acta Materialia, 2009, 57: 376−391.

[30] NELSON D R. Order, frustration, and defects in liquids and glasses [J]. Physical Review B, 1983, 28: 5515−5535.

[31] PAN S P, QIN J Y, WANG W M, GU T K. A new method to characterize medium range order in metallic glasses [J]. Journal of Non-Crystalline Solids, 2012, 358: 1873−1875.

[32] WEN D D, PENG P, JIANG Y Q, LIU R S. On the heredity and evolution of icosahedral clusters during the rapid solidification of liquid $Cu_{50}Zr_{50}$ alloys [J]. Journal of Non-Crystalline Solids, 2013, 378: 61−70.

[33] LAD K N, JAKSE N, PASTUREL A. Signatures of fragile-to-strong transition in a binary metallic glass-forming liquid [J]. The Journal of Chemical Physics, 2012, 136: 104509.

[34] TURNBULL D, COHEN M H. On the free-volume model of the liquid-glass transition [J]. The Journal of Chemical Physics, 1970, 52: 3038−3041.

冷却速度对快凝 $Cu_{56}Zr_{44}$ 合金二十面体团簇化的影响

胡艳军[1,2]，文大东[1]，蒋元祺[1]，邓永和[1]，彭 平[1]

1. 湖南大学 材料科学与工程学院，长沙 410082；
2. 广东医学院 信息工程学院，东莞 523808

摘 要：采用分子动力学方法模拟研究液态 $Cu_{56}Zr_{44}$ 合金不同冷速(γ)下的快速凝固过程。为了评估冷速对二十面体团簇化趋势与致密化程度的影响，采用十指数的团簇类型指数方法表征过冷液体和快凝固体的局域原子结构。利用二十面体团聚度(f_I)和化学序参数($\eta_{\alpha\beta}$)以及致密化系数(D_0，D_I 和 D_{IS})分别对其团簇化和有序度以及二十面体团簇密堆积度进行评估。结果表明，$Cu_{56}Zr_{44}$ 合金系统中主要的局域原子结构为 Cu 心的 Z12 团簇，其中大多数是(12 0 12 0 0 0 0 0 0 0)规则二十面体和(12 0 8 0 0 0 2 2 0 0) 及(12 2 8 2 0 0 0 0 0 0)缺陷二十面体。在 T_g 以下，二十面体基本团簇以 IS 铰链(二十面体键)结合成二十面体中程序(IMRO)，其数目 N、尺寸 n、序参数 $\eta_{\alpha\beta}$ 和空间分布随 γ 而变化。在玻璃转变的临界冷速 γ_c 以上，较低的冷速有利于二十面体数目的增加和 IMRO 尺寸的增大。同时，较慢的冷却过程有助于快凝固体中 IMRO 堆积密度的增加和二十面体团簇化程度的提高。

关键词：快速凝固；Cu−Zr 合金；冷却速度；团簇化；二十面体

(Edited by Xiang-qun LI)